ADVANCED ENGINEERING MATERIALS

COMMUNICATION

DOI: 10.1002/adem.201100116

Intrinsically Ductile Failure in a Nanocrystalline Beta Titanium Alloy**

By *Wei Xu,* Roberto B. Figueiredo, Xiaolin Wu, Simon Pauly, Mihai Stoica, Jürgen Eckert, Terence G. Langdon* and *Kenong Xia**

A nanocrystalline bcc $Ti_{67.4}Nb_{24.6}Zr_5Sn_3$ alloy is shown to fracture in an intrinsically ductile manner with exceptionally large dimples (up to 10 μm) which are two orders of magnitude greater than the grain size (≈ 40 nm). This large plasticity length scale is attributed to a combination of low shear modulus (≈ 27 GPa), high Poisson's ratio (≈ 0.4) and ultrahigh strength (UTS ≈ 1.1 GPa), close to the ideal shear stress, which facilitates ideal shear deformation to promote transgranular shear.

Nanocrystalline metals are exceptionally strong but generally fail with only limited ductility when crack growth is controlled by dislocation emission from the crack tips.[1] A number of approaches were developed toward the production of nanocrystalline metals that can withstand significant plastic strain before failure,[2–8] including creating a bimodal grain size distribution, generating profuse nano-twins, forming nano-precipitates, and modifying the stacking fault energy. From the fracture viewpoint, these strategies are designed to introduce structural heterogeneities that limit crack propagation during plastic deformation.

An alternative strategy that is not currently adopted in developing ductile nanocrystalline metals is based on the empirical correlation between ductility and the shear-to-bulk modulus ratio (G/B) which is inversely related to Poisson's ratio (ν).[9,10] It is well known that isotropic microcrystalline metals with high ν are generally more ductile by comparison to low-ν metals of the same crystal structure[9] in spite of the exception for B2 intermetallic compounds such as NiAl that has a high ν but is very brittle.[11] For an alloy system capable of forming bulk metallic glasses (BMGs), a brittle-to-ductile transition is also identified with increasing ν and BMGs with ν higher than ≈ 0.31–0.32 usually exhibit high toughness.[10] Moreover, Pan *et al.*[12] showed that the volume of the shear transformation zones (STZs) in BMGs and ductility increase with increasing ν, suggesting an intrinsic correlation between ductility and STZ volume. Nevertheless, no such correlation between ductility and ν has been explored in nanocrystalline metals and alloys.

On the fracture surface of a number of pure nanocrystalline metals, dimples are often observed with characteristic lengths of the order of ≈ 100 nm to 2 μm which is considerably larger than the grain size but smaller than in coarse-grained polycrystals.[3–5] Similarly, fracture analysis on BMGs[13] reveals the formation of dimples (vein pattern) and the fracture toughness is proposed to depend on the length scale of the dimples that corresponds to the plastic process zone. Accordingly, the larger the plastic process zone, the tougher the BMG. It appears that nanocrystalline metals also behave mechanically in a manner similar to BMGs with a susceptibility to shear banding.[14–16] For example, shear bands

[*] *Dr. W. Xu, Prof. K. Xia, Dr. X. Wu*
Department of Mechanical Engineering and ARC Centre of Excellence for Design in Light Metals
University of Melbourne, Victoria 3010, (Australia)
E-mail: weixu@unimelb.edu.au; k.xia@unimelb.edu.au
Dr. R. B. Figueiredo
Department of Metallurgical and Materials Engineering, Federal University of Minas Gerais
Belo Horizonte, MG 31270-901, (Brazil)
Dr. S. Pauly, Dr. M. Stoica, Prof. J. Eckert
Institut für Komplexe Materialien, IFW Dresden, Helmholtzstraße 20
D-01069 Dresden, (Germany)
Prof. J. Eckert
Institut für Werkstoffwissenschaft, TU Dresden
D-01062 Dresden, (Germany)
Prof. T. G. Langdon
Materials Research Group, School of Engineering Sciences
University of Southampton, Southampton SO17 1BJ, (UK)
Prof. T. G. Langdon
Departments of Aerospace and Mechanical Engineering and Materials Science, University of Southern California
Los Angeles, CA 90089-1453, (USA)

[**] *Support is gratefully acknowledged from the Australian Research Council, the AvH Foundation, the German Science Foundation, and the National Science Foundation of the United States (Grant No. DMR-0855009).*
This paper was amended in issue 12 of Advanced Engineering Materials because of wrong affiliations of Prof. Langdon in the Early View publication.

develop immediately after the onset of plastic deformation in nanocrystalline bcc Fe.[14] These similarities raise the question of whether a high-ν nanocrystalline alloy is intrinsically ductile and it is of interest to identify the nature of the associated deformation mechanism to fracture.

In this study, a high-ν beta titanium alloy ($Ti_{67.4}Nb_{24.6}Zr_5Sn_3$, at%) with an electron/atom ratio (e/a) of 4.24 was processed by the following routes to attain different grain sizes: (i) solution treatment (ST), (ii) ST plus equal-channel angular pressing (ECAP), and (iii) ST plus high-pressure torsion (HPT). The corresponding microstructures had grain sizes of different scales: micro (Micro-TNZS, ST), ultrafine (UFG-TNZS, ECAP) and nano (Nano-TNZS, HPT) with average grain sizes, d, of $\approx 200 \pm 50\,\mu m$, $\approx 410 \pm 130\,nm$, and $\approx 40 \pm 15\,nm$, respectively.

Results and Discussion

For the elastic properties (Table 1), all materials display ν close to 0.4 and the slight variation in Young's modulus (E) and G for UFG-TNZS is due to the presence of a small amount (< 1 vol%) of athermal ω and α'' phases.[17] In terms of the mechanical properties, there are no significant effects from these small amounts of secondary phases. Nano-TNZS shows enhanced yield strength ($\approx 920\,MPa$) and ultimate tensile strength (UTS, $\approx 1100\,MPa$) doubling that for Micro-TNZS (≈ 445 and $576\,MPa$, respectively) with a reduced but appreciable elongation to failure ($\approx 5\%$). The UTS/E ratio of 0.015 for Nano-TNZS is higher than values up to ≈ 0.011 for conventional crystalline materials and approaches the value of 0.018 for a nanocrystalline Fe–Ni–Co–Ti alloy.[18] A high UTS/E ratio implies limited activities of lattice dislocations due to the high propensity for ideal shear deformation.[18]

The fracture surfaces of Micro-TNZS and UFG-TNZS exhibit large, deep and irregular dimples (Fig. 1a and b) indicating a typical ductile fracture, whereas deformation of Nano-TNZS yields a distinct fracture surface (Fig. 1c) with equiaxed dimples up to $\approx 10\,\mu m$ in size. The average dimple size (D) in Nano-TNZS is $\approx 2 \pm 1.6\,\mu m$. However, the area fraction of dimples larger than $2\,\mu m$ is about 86%, and the average size of these large dimples is $\approx 4.5 \pm 1.1\,\mu m$ which is two orders of magnitude greater than the average grain size. The depth of these large dimples is estimated using SEM/FIB analysis as about 2–3 μm.

By examining individual dimples, nanoscale features are clearly visible across the dimple in Nano-TNZS (Fig. 1d). Closer examination reveals some difference between the nanoscale features on the thin ridge between dimples (Fig. 1e) and inside the dimple (Fig. 1f). The peripheral rim of the dimple is composed of 1–2 rows of undeformed equiaxed nano-grains, whereas toward the center the nanoscale features are flat and the grains are less recognizable and appear clustered. Near the dimple bottom (Fig. 1f), visible nanocracks are interlocked at grain cluster interfaces, providing indirect evidence for the presence of cooperative shearing clusters as predicted by Hasnaoui *et al*.[19]

Table 1. Elastic properties of bcc $Ti_{67.4}Nb_{24.6}Zr_5Sn_3$ beta alloy.

Elastic properties	Micro-TNZS	UFG-TNZS	Nano-TNZS
Young's modulus, E [GPa]	77 ± 1	81 ± 1	76 ± 1
Shear modulus, G [GPa]	28 ± 1	29 ± 1	27 ± 1
Bulk modulus, B [GPa]	127 ± 1	118 ± 1	122 ± 3
Poisson's ratio, ν	0.399	0.385	0.396

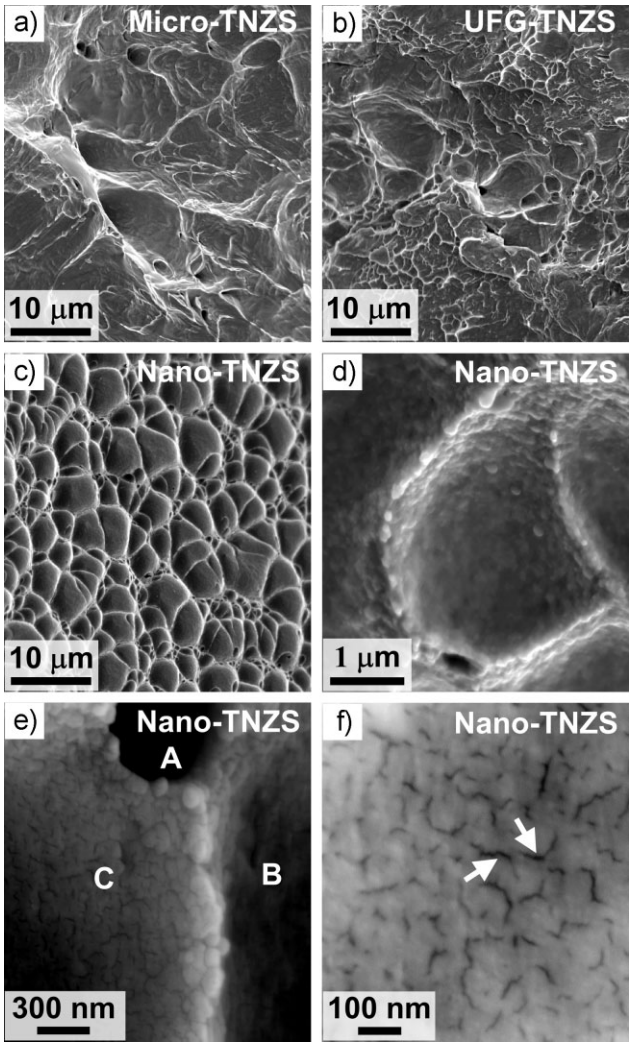

Fig. 1. Tensile fracture surfaces (SEM) of $Ti_{67.4}Nb_{24.6}Zr_5Sn_3$. (a, b) Micro-TNZS and UFG-TNZS show dimpled features similar to that observed in ductile microcrystalline metals. (c) Nano-TNZS displays large equiaxed dimples two orders of magnitude larger than the average grain size. (d) Nano-TNZS shows nanoscale features across the entire dimple. (e) The peripheral rims of the dimples (A–C) in Nano-TNZS are composed of 1, 2 rows of undeformed equiaxed nano-grains. (f) Visible nanocracks in Nano-TNZS are interlocked at interfaces of nanoscale grain clusters.

Vickers indentation analysis also showed distinct deformation features. Micro-TNZS and UFG-TNZS exhibited pile-up indentations and deformed primarily by dislocation-mediated plasticity with sets of slip lines spreading out around the indentations (Fig. 2a and b). However, the area around the sink-in indentation in Nano-TNZS is featureless without any visible slip lines or shear bands (Fig. 2c). As shear banding is a sign of localized plastic deformation,[14] the absence of shear

COMMUNICATION

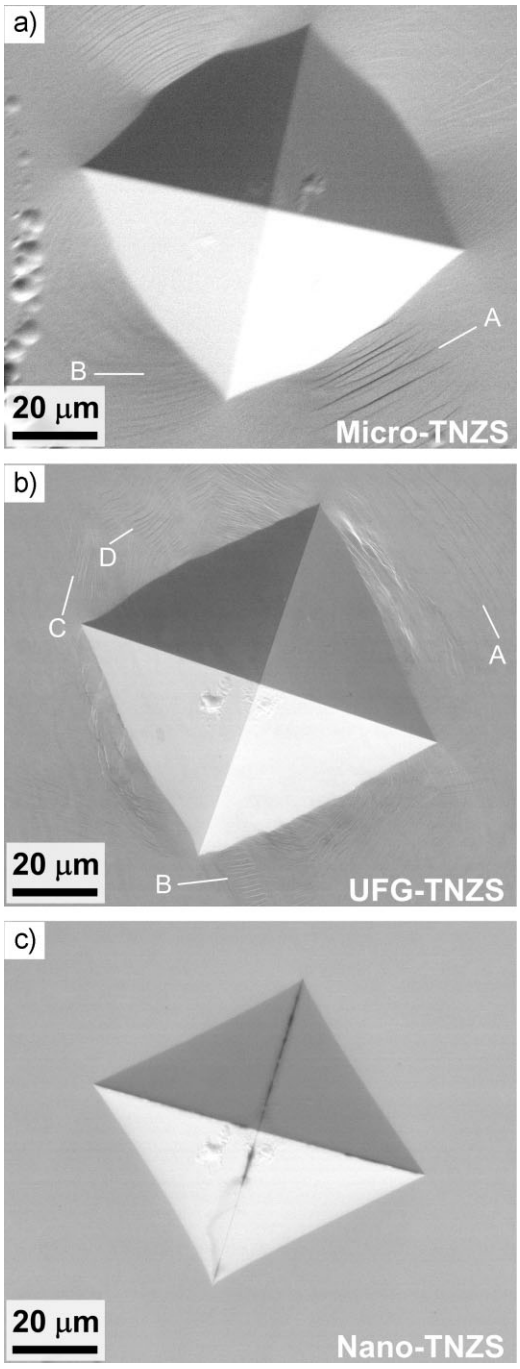

Fig. 2. Vickers indentations of $Ti_{67.4}Nb_{24.6}Zr_5Sn_3$. (a) Sets of dislocation slip lines (A, B) spread out around an indentation in Micro-TNZS. (b) Both slip lines (A–D) and shear bands are visible around an indentation in UFG-TNZS. (c) Neither slip lines nor shear bands are present surrounding an indentation in Nano-TNZS.

bands in Nano-TNZS indicates an increased resistance to shear localization and this is different from nanocrystalline Fe ($\nu = 0.293$) which exhibits pile-up indentations with shear bands.[15]

Dimpled fracture has been identified in a number of nanocrystalline metals[3–5,19] featuring dimples with an average size (≈ 100 nm–2 μm) one order of magnitude larger than the grain size. There are numerous attempts to explain the dimple fracture in nanocrystalline metals. Kumar *et al.*[3] proposed a model giving intragranular fracture dimples through a coupling of dislocation-mediated plasticity and unaccommodated grain boundary sliding. A molecular dynamics simulation[19] showed that grain boundary sliding and partial dislocation activity may lead to the formation of local shear planes that span several grains, thereby creating cooperative shearing clusters. It was suggested that the length scale of these clusters determined the dimple dimension. Recently, the presence of such grain clusters was evident in TEM analysis during tensile straining in which cracks were observed to propagate in a combined inter- and intra-agglomerate deformation manner.[20]

On the other hand, large dimples as in the present case were reported only in a uniform nanocrystalline Fe–Ni–Co–Ti alloy[18] (the detailed features of the fracture surface were not shown) and a nanocrystalline Cu with bundles of nanoscale twins.[21] However, the presence of microscale deformation twin bundles may account for the formation of dimples as large as tens of micrometers in the nanocrystalline Cu, which is in striking contrast to that of several hundred nanometers found in a uniform nanocrystalline Cu.[22] Based on available data, Table 2 summarizes the dimple and grain sizes observed in a number of uniform nanocrystalline metals and alloys (Ni,[3,5,23] Cu,[22] Pd,[8] Fe,[24] Fe–Ni–Co–Ti,[18] and the present Nano-TNZS), indicating that the large dimples observed in Nano-TNZS and Fe–Ni–Co–Ti are exceptional compared to nanocrystalline pure metals.

It was proposed that the nanocrystalline Fe–Ni–Co–Ti may deform at a strength near its ideal strength,[18] similar to that reported in the ''Gum metal'' (GM),[25–29] a class of bcc beta-Ti alloys. Interestingly, a detailed examination shows that Nano-TNZS, Nano-FeNiCoTi and GM share the following common characteristics: low G, high ν and ultrahigh strength. In bcc and fcc metals (Fig. 3a), lower G is beneficial to attain lower ideal shear strength, $\tau_{max} \approx 0.11G_{111} = 0.11 \times 3(c_{11}-c_{12})[5G-(c_{11}-c_{12})]/[20G-(c_{11}-c_{12})]$[26,30] at fixed c_{11}–c_{12}, where c_{11} and c_{12} are elastic constants, and G_{111} is shear modulus along <111> direction. The GM is reported to have τ_{max} of 1.7–1.9 GPa based on the measured G of 20 GPa[26] and the calculated c_{11}–c_{12} of 25–27 GPa.[28] The nanocrystalline Fe–Ni–Co–Ti is reported to have similar elastic constants as

Table 2. Measured dimple and grain size in uniform nanocrystalline metals and alloys.

Pure metals or alloys	Grain size d [nm]	Dimple size D [μm]	D/d	Ref.
Cu	23	0.23 ± 0.14	≈ 10	[22]
Ni[a]	30	0.24 ± 0.05	≈ 8	[3]
Ni[b]	44	1.21 ± 0.5	≈ 28	[5]
Ni[c]	29	0.56 ± 0.12	≈ 19	[23]
Pd	240	≈ 7.2	≈ 30	[8]
Fe	33	0.24 ± 0.06	≈ 7	[24]
Nano-TNZS	40 ± 15	4.5 ± 1.1	≈ 113	Present
Fe–Ni–Co–Ti	20–50	7.4 ± 1.5	≈ 200	[18]

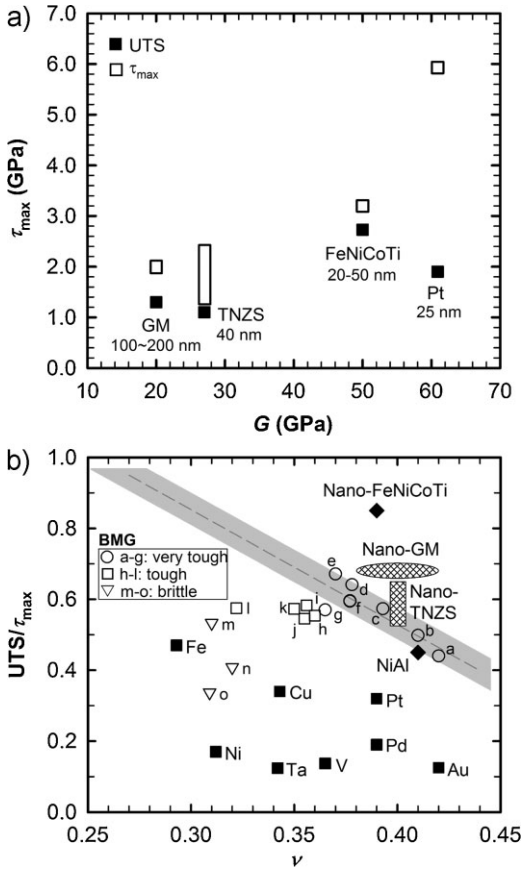

Fig. 3. (a) Measured UTS and calculated ideal shear strength (τ_{max}) are shown for Nano-TNZS and nanocrystalline Fe–Ni–Co–Ti, ''Gum metal'' and Pt. (b) A ν–UTS/$\hat{o}_{max}$ map for a number of nanocrystalline/ultrafine-grained pure metals such as Fe,[24] Ta,[37] V,[38] Ni,[5] Cu,[22] Pt,[34] Pd,[8] and Au,[39] nanocrystalline intermetallic compounds such as NiAl,[35] Nano-TNZS, nanocrystalline Fe–Ni–Co–Ti,[18,31] and ''Gum metal.''[25–29] A number of tough and brittle BMGs are presented for comparison.(a-$Pt_{57.5}Cu_{14.7}Ni_{5.3}P_{22.5}$,[40] b-$Pd_{77.5}Cu_6Si_{16.5}$,[10,13] c-$Zr_{70}Ni_{16}Cu_6Al_8$,[41] d-$Zr_{62}Cu_{15.5}Ni_{12.5}Al_{10}$,[42] e-$Ti_{40}Zr_{25}Cu_{12}Ni_3Be_{20}$,[43] f-$Zr_{61.88}Cu_{18}Ni_{10.12}Al_{10}$,[42] g-$Cu_{47.5}Zr_{47.5}Al_5$,[44] h-$Zr_{41}Ti_{14}Cu_{12.5}Ni_{10}Be_{22.5}$,[45] i-$Ti_{55}Zr_{10}Cu_9Ni_8Be_{18}$,[46] j-$Zr_{65}Cu_{15}Ni_{10}Al_{10}$,[42,47] k-$Cu_{50}Zr_{50}$,[44] l-$Fe_{64.85}Mo_{14}C_{15}B_6Er_{0.15}$,[48] m-$Fe_{48}Cr_{15}Mo_{14}Er_2C_{15}B_6$,[48,49] n-$Ce_{70}Al_{10}Cu_{20}$,[50] o-$Mg_{65}Cu_{25}Tb_{10}$[13]).

Fe-36.5 at% Ni, which yields τ_{max} of 3.2 GPa.[31] On the basis of Fe-36.5 at% Ni, the values of G and ν for Fe–Ni–Co–Ti may also be reasonably estimated to be about 50 GPa and 0.39.[32] On the other hand, Nano-TNZS with an e/a of 4.24 may have similar elastic constants (c_{11}, c_{12}, and c_{44}) to that for Ti-25 at% Nb[33] and c_{11}–c_{12} for Nano-TNZS is estimated to be in the range between 15 and 30 GPa, which yields τ_{max} not more than 2 GPa. Apparently, the attained UTS for Nano-TNZS (1.1 GPa), nanocrystalline Fe–Ni–Co–Ti (2.73 GPa)[18] and nanocrystalline GM (1.3 GPa)[29] approaches their corresponding τ_{max}, which is in striking contrast to a nanocrystalline Pt[34] (25 nm) with UTS of 1.9 GPa which is far below its τ_{max} of about 5.9 GPa. As suggested for Fe–Ni–Co–Ti[18,31] and GM,[25–29] Nano-TNZS should have high propensity to experience ideal shear deformation when local stress concentration is present.

To clearly address the effect of Poisson's ratio and high propensity for ideal shear deformation on the formation of large dimples, a map of ν–UTS/τ_{max} is constructed in Figure 3b composed of a number of nanocrystalline pure metals, intermetallic compounds such as NiAl,[35] Nano-TNZS, nanocrystalline Fe–Ni–Co–Ti, and GM. The Poisson's ratio for GM, although not previously reported, can be estimated as in the range between 0.38 and 0.42 from available elastic constants reported in the literature.[25–29] For comparison, a number of BMGs are also shown in Figure 3b by using the maximum compressive strength (true stress) to replace UTS and $G/10$ as the ideal shear strength that is recently determined by molecular dynamics simulation.[36] Interestingly, UTS/τ_{max} for those very tough/ductile BMGs is in linear proportion to ν. As proposed by Pan *et al.*,[12] these BMGs with higher ν should have larger STZ volume which enhances the capability for shear deformation and leads to multiple shear banding. In addition, according to Xi *et al.*[13] these very tough/ductile BMGs may show large-scale plastic process zone (dimple), and vice versa. As a result, an upper boundary (shaded area in Fig. 3b) is established for BMGs in the ν–UTS/τ_{max} map. BMGs with ν and UTS/τ_{max} close to the boundary are very tough/ductile with large dimples formed on fracture surface and toward the lower left-hand corner of the ν–UTS/τ_{max} map the BMGs become less ductile and eventually brittle with very fine dimples.

Surprisingly, Nano-TNZS and nanocrystalline Fe–Ni–Co–Ti with exceptional large dimples (i.e., dimples two orders of magnitude larger than the grain size) are noted together with nanocrystalline GM to locate above the upper boundary defined in the ν–UTS/τ_{max} map. On the other hand, values of ν and UTS/τ_{max} are far below the boundary for those nanocrystalline pure metals with dimples one order of magnitude larger than the grain size. Important implications from Figure 3b are that the length scale of dimples in nanocrystalline metals and alloys may depend on both ν and UTS/τ_{max}, and a material with higher ν requires lower UTS/τ_{max} to initiate ideal shear deformation. Nevertheless, it seems very difficult for nanocrystalline pure metals to attain both high ν and UTS/τ_{max} near the defined boundary only by means of grain refinement. For low-ν pure metals such as Fe,[24] although the attained UTS is as high as one-half of its ideal shear strength, it is still much lower than the required strength for ideal shear deformation. Similarly, for high-ν pure metals such as Pt,[34] it is also not feasible to further dramatically enhance strength by grain refinement to approach the boundary since the average grain size for Pt is already as fine as 25 nm. To attain both high ν and high UTS/τ_{max}, a more practical approach is to appropriately design alloys with low G and high ν, and to dramatically refine the grains to attain ultrahigh strength, such as in the case of nanocrystalline Fe–Ni–Co–Ti, GM, and Nano-TNZS.

Based on the ν–UTS/τ_{max} map, the formation of dimples in nanocrystalline metals and alloys may be understood by considering three competing deformation mechanisms: conventional slip of lattice dislocations, grain boundary sliding and ideal shear deformation. At low UTS/τ_{max}, an ultrafine-grained material may deform by conventional slip of

lattice dislocations. Toward higher UTS/τ_{max}, slip of lattice dislocations is gradually suppressed and grain boundary-mediated deformation such as grain boundary sliding becomes prevalent until the initiation of ideal shear deformation. The key role of high ν and low G is to reduce the resistance to shear deformation, and thus promote grain boundary sliding and make ideal shear deformation more viable when local stress exceeds the ideal strength. As previously stated,[3,19] the size of cooperative shearing clusters created during grain boundary sliding and partial dislocation activity may determine the dimple dimension in nanocrystalline materials. This largely represents the case of low and medium UTS/τ_{max} for nanocrystalline pure metals with dimples that span up to tens of grains. Nevertheless, the process of grain boundary sliding is still controlled by the nucleation and glide of partial grain boundary dislocations,[1] which is believed to limit the size of cooperative shearing clusters and therefore the dimple dimension with only marginal variation. This may account for the lack of strong dependency of dimple size on ν for nanocrystalline pure metals.

On the other hand, it is a different scenario for nanocrystalline alloys with both high ν and UTS/τ_{max} (Nano-TNZS and Fe–Ni–Co–Ti). At low applied stress, grain boundary sliding may be operative but is confined at a scale equivalent to the dimension of the cooperative shearing clusters which span several to tens of grains. With increasing stress, ideal shear deformation becomes predominant, in particular at local regions with stress concentrations exceeding ideal shear stress. As a result, transgranular shear may proceed at a much larger scale along the maximum shear stress plane without the aid of any dislocations, which is believed to lead to the formation of the large dimples in Nano-TNZS and the nanocrystalline Fe–Ni–Co–Ti. Accordingly, a nanocrystalline alloy with low shear modulus, high Poisson's ratio and ultrahigh strength, is suggested to be intrinsically ductile, which opens a new perspective for developing ductile nanocrystalline metallic alloys.

Conclusions

A unique ductile fracture surface was found in a nanocrystalline $Ti_{67.4}Nb_{24.6}Zr_5Sn_3$ beta alloy with G of 27 GPa, high ν of 0.4, and high UTS of 1.1 GPa, exhibiting uniform and large dimples that are two orders of magnitude greater than the average grain size. Based on a number of nanocrystalline materials and BMGs, a ν–UTS/τ_{max} map was constructed to elucidate the underlying deformation mechanism for the formation of large dimples in Nano-TNZS. It is revealed that low shear modulus, high Poisson's ratio and ultrahigh strength may facilitate ideal shear deformation to promote transgranular shear, leading to the intrinsically ductile failure in Nano-TNZS. These findings suggest a new and alternative approach for exploring the characteristics of inherently ductile nanocrystalline alloys.

Experimental

Materials Processing

The $Ti_{67.4}Nb_{24.6}Zr_5Sn_3$ (at%) alloy was prepared by arc-melting a mixture of high purity elements (99.99%) under Ar, followed by cold crucible casting and subsequent solution treatment at 1273 K for 24 h. Cylindrical rods of 40 mm in length and 10 mm in diameter were processed using C-route ECAP (sample rotation by 180° between passes) at 903 K for four passes and disks of 0.8 mm in thickness and 10 mm in diameter were processed by HPT at room temperature under 6 GPa for five revolutions.

Characterization

The elastic constants were determined by ultrasonic sound velocity measurements (Olympus Panametrics-NDT 5900PR). Dog-bone-shaped tensile specimens (gauge length: 2 mm; width: 1 mm; thickness: Micro-TNZS $\approx$0.41 mm, UFG-TNZS $\approx$0.40 mm, Nano-TNZS $\approx$0.22 mm) were tested at room temperature with an initial strain rate of 1.0×10^{-2} s^{-1}. Vickers indentation was performed under a static load of 1 000 g for 15 s. Microstructure and fracture analyses were carried out using optical microscopy and scanning electron microscopy (SEM, FEI Quanta 200F).

Received: April 18, 2011
Final Version: May 30, 2011
Published online: June 30, 2011

[1] I. A. Ovid'ko, A. G. Sheinerman, *Acta Mater.* **2010**, *58*, 5286.
[2] Y. M. Wang, M. W. Chen, F. H. Zhou, E. Ma, *Nature* **2002**, *419*, 912.
[3] K. S. Kumar, S. Suresh, M. F. Chisholm, J. A. Horton, P. Wang, *Acta Mater.* **2003**, *51*, 387.
[4] K. M. Youssef, R. O. Scattergood, K. L. Murty, C. C. Koch, *Appl. Phys. Lett.* **2004**, *85*, 929.
[5] H. Q. Li, F. Ebrahimi, *Appl. Phys. Lett.* **2004**, *84*, 4307.
[6] E. Ma, Y. M. Wang, Q. H. Lu, M. L. Sui, L. Lu, K. Lu, *Appl. Phys. Lett.* **2004**, *85*, 4932.
[7] Z. Horita, K. Ohashi, T. Fujita, K. Kaneko, T. G. Langdon, *Adv. Mater.* **2005**, *17*, 1599.
[8] K. Yang, Y. Ivanisenko, A. Caron, A. Chuvilin, L. Kurmanaeva, T. Scherer, R. Z. Valiev, H. J. Fecht, *Acta Mater.* **2010**, *58*, 967.
[9] S. F. Pugh, *Philos. Mag.* **1954**, *45*, 823.
[10] J. J. Lewandowski, W. H. Wang, A. L. Greer, *Philos. Mag. Lett.* **2005**, *85*, 77.
[11] K. Gschneidner, A. Russell, A. Pecharsky, J. Morris, Z. Zhang, T. Lograsso, D. Hsu, C. Lo, Y. Ye, A. Slager, D. Kesse, *Nat. Mater.* **2003**, *2*, 587.
[12] D. Pan, A. Inoue, T. Sakurai, M. W. Chen, *PNAS* **2008**, *105*, 14769.
[13] X. K. Xi, D. Q. Zhao, M. X. Pan, W. H. Wang, Y. Wu, J. J. Lewandowski, *Phys. Rev. Lett.* **2005**, *94*, 125510.
[14] D. Jia, K. T. Ramesh, E. Ma, *Acta Mater.* **2003**, *51*, 3495.

[15] T. R. Malow, C. C. Koch, P. Q. Miraglia, K. L. Murty, *Mater. Sci. Eng, A* **1998**, *252*, 36.
[16] C. A. Schuh, T. C. Hufnagel, U. Ramamurty, *Acta Mater.* **2007**, *55*, 4067.
[17] W. Xu, X. Wu, M. Calin, M. Stoica, J. Eckert, K. Xia, *Scr. Mater.* **2009**, *60*, 1012.
[18] S. Kuramoto, T. Furuta, N. Nagasako, Z. Horita, *Appl. Phys. Lett.* **2009**, *95*, 211901.
[19] A. Hasnaoui, H. Van Swygenhoven, P. M. Derlet, *Science* **2003**, *300*, 1550.
[20] Z. W. Shan, J. A. Knapp, D. M. Follstaedt, E. A. Stach, J. M. K. Wiezorek, S. X. Mao, *Phys. Rev. Lett.* **2008**, *100*, 105502.
[21] E. W. Qin, L. Lu, N. R. Tao, J. Tan, K. Lu, *Acta Mater.* **2009**, *57*, 6215.
[22] R. K. Guduru, K. L. Murty, K. M. Youssef, R. O. Scattergood, C. C. Koch, *Mater. Sci. Eng, A* **2007**, *463*, 14.
[23] Y. M. Wang, S. Cheng, Q. M. Wei, E. Ma, T. G. Nieh, A. Hamza, *Scr. Mater.* **2004**, *51*, 1023.
[24] T. R. Malow, C. C. Koch, *Metall. Mater. Trans. A* **1998**, *29*, 2285.
[25] T. Saito, T. Furuta, J. H. Hwang, S. Kuramoto, K. Nishino, N. Suzuki, R. Chen, A. Yamada, K. Ito, Y. Seno, T. Nonaka, H. Ikehata, N. Nagasako, C. Iwamoto, Y. Ikuhara, T. Sakuma, *Science* **2003**, *300*, 464.
[26] S. Kuramoto, T. Furuta, J. H. Hwang, K. Nishino, T. Saito, *Metall. Mater. Trans. A* **2006**, *37*, 657.
[27] T. Li, J. W. Morris, N. Nagasako, S. Kuramoto, D. C. Chrzan, *Phys. Rev. Lett.* **2007**, *98*, 105503.
[28] M. Hara, Y. Shimizu, T. Yano, N. Takesue, T. Furuta, S. Kuramoto, *Int. J. Mater. Res.* **2009**, *100*, 345.
[29] T. Furuta, M. Hara, Z. Horita, S. Kuramoto, *Int. J. Mater. Res.* **2009**, *100*, 1217.
[30] C. R. Krenn, D. Roundy, J. W. Morris, M. L. Cohen, *Mater. Sci. Eng, A* **2001**, *319*, 111.
[31] T. Furuta, S. Kuramoto, K. Horibuchi, T. Ohsuna, Z. Horita, *J. Mater. Sci.* **2010**, *45*, 4745.
[32] O. Yeheskel, *Metall. Mater. Trans. A* **2009**, *40*, 684.
[33] H. Ikehata, N. Nagasako, T. Furuta, A. Fukumoto, K. Miwa, T. Saito, *Phys. Rev. B* **2004**, *70*, 174113.
[34] K. N. Jonnalagadda, I. Chasiotis, S. Yagnamurthy, J. Lambros, J. Pulskamp, R. Polcawich, M. Dubey, *Exp. Mech.* **2010**, *50*, 25.
[35] M. S. Choudry, M. Dollar, J. A. Eastman, *Mater. Sci. Eng, A* **1998**, *256*, 25.
[36] Y. Q. Cheng, E. Ma, *Acta Mater.* **2011**, *59*, 1800.
[37] S. N. Mathaudhu, K. T. Hartwig, *Mater. Sci. Eng, A* **2007**, *463*, 94.
[38] Z. Z. Jiang, S. H. Yu, Y. B. Chun, D. H. Shin, S. K. Hwang, *Mater. Sci. Eng, A* **2008**, *479*, 285.
[39] T. Suzuki, A. Vinogradov, S. Hashimoto, *Mater. Trans.* **2004**, *45*, 2200.
[40] J. Schroers, W. L. Johnson, *Phys. Rev. Lett.* **2004**, *93*, 255506.
[41] Y. Yokoyama, K. Fujita, A. R. Yavari, A. Inoue, *Philos. Mag. Lett.* **2009**, *89*, 322.
[42] Y. H. Liu, G. Wang, R. J. Wang, D. Q. Zhao, M. X. Pan, W. H. Wang, *Science* **2007**, *315*, 1385.
[43] X. J. Gu, S. J. Poon, G. J. Shiflet, J. J. Lewandowski, *Acta Mater.* **2010**, *58*, 1708.
[44] J. Das, M. B. Tang, K. B. Kim, R. Theissmann, F. Baier, W. H. Wang, J. Eckert, *Phys. Rev. Lett.* **2005**, *94*, 205501.
[45] R. D. Conner, A. J. Rosakis, W. L. Johnson, D. M. Owen, *Scr. Mater.* **1997**, *37*, 1373.
[46] J. M. Park, G. Wang, S. Pauly, N. Mattern, D. H. Kim, J. Eckert, *Metall. Mater. Trans. A* **2011**, *42*, 1456.
[47] H. Bei, Z. P. Lu, S. Shim, G. Chen, E. P. George, *Metall. Mater. Trans. A* **2010**, *41*, 1735.
[48] X. J. Gu, A. G. McDermott, S. J. Poon, *Appl. Phys. Lett.* **2006**, *88*, 211905.
[49] V. Ponnambalam, S. J. Poon, G. J. Shiflet, *J. Mater. Res.* **2004**, *19*, 1320.
[50] B. Zhang, D. Q. Zhao, M. X. Pan, W. H. Wang, A. L. Greer, *Phys. Rev. Lett.* **2005**, *94*, 205502.

